Investigation of the Protection Performance of Mg and Al Coated Copper in High Temperature or Marine Environments

Dimitrios Stathokostopoulos [1], Christos A. Vogiatzis [2], Konstantinos Chrissafis [1], Stefanos Skolianos [2], George Vourlias [1] and Dimitrios Chaliampalias [1,*]

[1] Physics Department, Aristotle University of Thessaloniki, 54124 Thessaloniki, Greece; dstat@physics.auth.gr (D.S.); hrisafis@physics.auth.gr (K.C.); gvourlia@auth.gr (G.V.)

[2] Department of Mechanical Engineering, Aristotle University of Thessaloniki, 54124 Thessaloniki, Greece; chvogia@gmail.com (C.A.V.); skol@auth.gr (S.S.)

* Correspondence: dimchal@auth.gr; Tel.: +30-693-617-9336

Abstract: Copper is commonly used in many applications such as electric wires, industrial machinery, boat propellers and heat exchangers. Although Cu is resistant to corrosion in ambient conditions, it is highly susceptible when exposed to harsh environments such as high-temperature air or marine atmospheres. The application of magnesium or aluminum coatings on Cu can efficiently smooth this disadvantage without affecting its primer properties. In the herein investigation, the deposition of these coatings was accomplished by pack cementation, a simple electrochemical technique which can be easily incorporated in the industrial scale. The final coatings were tested under high temperature environments by non-isothermal (dynamic) and isothermal thermogravimetric measurements, and in artificial sea water (3.5 wt.%-NaCl) by electrochemical corrosion. The structure of both coatings was compact with elevated thickness. The oxidation and corrosion measurements revealed that the coated samples had much better performance compared to the uncoated copper coupons. Furthermore, Al coatings were found to have the best performance when exposed in high temperature environment.

Keywords: pack cementation; protective coatings; electrochemical corrosion; high temperature oxidation; XRD; thermal analysis

1. Introduction

Copper, due to its characteristics, is one of the most common materials for a variety of applications such as electrical wires, industrial machinery, boat propellers and heat exchangers [1,2]. The wide use of copper can be attributed to its properties such as excellent thermal and electrical conductivity, ductility and malleability. Due to its importance, the corrosion of this metal has been studied for a long time. Copper's corrosion resistance is attributed to the formation of a protective film of cuprous oxide (Cu_2O and CuO) [3]. This film retards both the anodic dissolution of the metal and the rate of O_2 reduction, meaning that any failure is associated with the deterioration of that film, depending on the environmental conditions. Particularly, copper is more susceptible to the presence of chlorides, sulfur and applied fields [4]. Furthermore, a typical copper corrosion could be caused by the presence of the organic decomposition products on the surface leading to the formation of carboxylic acid [5].

The application of protective coatings is an ideal method for enhancing the corrosion resistance of copper against different corrosion types—environments—(e.g., high temperature oxidation, corrosion in seawater). These coatings can be of a polymer type [4,6,7] or metallic made from zinc, chromium, magnesium and aluminum. Magnesium and aluminum are two good candidates that can be used for the corrosion and oxidation protection of copper [8]. Magnesium is preferred as coating material on copper compo-

nents because it does not affect significantly the beneficial electric properties of Cu, whereas aluminum coatings have good oxidation resistance at high temperatures due to the formation of a thin Al_2O_3 layer which is an efficient diffusion barrier [9]. Up to now the formation of Cu-Mg and Cu-Al phases are investigated either in form of coating or in form of bulk alloy. Suwwan de Felipeet et al. [10] refer the co-deposition of both phases by magnetron sputtering, which improved the high temperature corrosion without affecting significantly the Cu ion mobility. The same conclusion is reported by Arcot et al. [11], who found that the Mg deposition with Cu had low electric resistivity, which makes it ideal for wire protection. Zhu et al. [12] examined the effect of Mg/Al alloying of copper by plasma arc melting and found that both elements improve the oxidation resistance up to 400 °C, with the Al alloyed samples having the best performance. Zhao et al. [13] investigated the Mg implantation on Cu by a high current ion source and found improvement of oxidation resistance at 300 °C without any noticeable influence on the electric conductivity. Aluminizing of copper is referred to have been accomplished by high temperature diffusion procedures [14–17], Cathodic arc plasma and sputtering [18,19] or hot pressing [20]. Al was found to provide significant long-term protection to copper up to 800–900 °C, depending on the Al concentration, mainly by the formation of Al_2O_3.

A promising, simple and low-cost technique for the formation of Cu-Mg and Cu-Al phases is chemical vapor deposition with pack cementation process, as the energy consumption during pack cementation is much lower than other techniques and it is environment-friendly due to the lack of polluting byproducts. Moreover, a major asset of this procedure is the formation of homogeneous coatings over irregularly shaped objects [21,22].

Pack aluminization of copper is reported only by Chiang et al. and Shi et al., who deposited Al at high temperatures (over 800 °C) and for holding times over 4 h. Magnesium deposition is mainly referred by physical vapor procedures [10–12,23]. Furthermore, the oxidation and corrosion performance of the final products is not investigated in a wide range of temperatures or in marine environments. The aim of this study is to investigate the deposition and structure of magnesium and aluminum coatings on copper by pack cementation at low temperatures and holding times, and examine the high temperature oxidation and corrosion performance of the final products by thermal analysis and electrochemical corrosion, respectively. The characterization of the coatings was performed using Scanning Electron Microscopy (SEM) and X-ray diffraction (XRD) analysis, while high temperature oxidation and corrosion tests were examined by dynamic/isothermal oxidations and exposure in simulated seawater solution.

2. Materials and Methods

The substrates that were used for the experimental process had dimensions 6 mm ×4 mm × 2 mm and were cut from C10800 copper alloy. Before the coating process, the substrates were suitably prepared by ultrasonic cleaning and mechanical polishing using up to 1000-grid SiC paper. Finally, the substrates were thoroughly cleaned in alcohol solution. The as prepared substrates were buried in a powder mixture consisting of 25 and 28 wt.% magnesium (Mg) and aluminum (Al) powder, respectively, 3 wt.% ammonium chloride (NH_4Cl) and balance aluminum oxide (Al_2O_3). These mixtures were found to be optimum for such coatings as reported in previous published work [24,25]. Mg/Al was the donor material, NH_4Cl the halide activator and Al_2O_3 the inert filler. The mixture with the substrate was then packed and sealed in ceramic crucibles and inserted in an Ar purged furnace preheated at the deposition temperature. The experimental conditions for the deposition procedures were: temperature of heat treatment 550 °C and holding time 2 h for both Mg and Al deposition. After the 2 h coating the system was left to cool down to ambient temperature without interrupting the Ar flow. Afterwards, the coated samples were cleaned from the remaining powder on their surface and metallograph-

ically prepared for microscopic observation by mechanical polishing using up to 2000-grid SiC paper and Al_2O_3 paste (5 μm), and extensive cleaning in alcoholic solution.

The coated samples were examined by two different tests which corresponded to high temperature and marine corrosive environments. The examination of the high temperature oxidation resistance of the specimens was accomplished through dynamic thermogravimetric measurements (TG) from ambient temperature up to 1000 °C carried in a TG-DTA SetaramSetsys 16/18 system (SETSYS, Lyon, France), with heating rate 10 °C/min and air flow 50 mL per minute. Furthermore, isothermal thermogravimetric measurements were also performed at selective temperatures in order to evaluate the durability of the samples. Four different oxidation temperatures were implemented for each coating: 550, 600, 650 and 700 °C for Mg coatings and 800, 850, 900 and 950 °C for Al coatings, and the holding time was6 h. During these tests, the mass gain vs. temperature, for dynamic oxidations, and the mass gain vs. time, for isothermal oxidations, were recorded for the evaluation of the samples.

The performance in marine atmosphere was evaluated through electrochemical corrosion experiments using a conventional three-electrode cell in 3.5 wt.% NaCl aqueous (distilled water) solution at room temperature (~25 °C). The reproducibility of the electrochemical test was verified by carrying out three measurements for each sample. Prior to potentiodynamic polarization, the working electrode was immersed into the test solution at open circuit potential (OCP) for 60 min to attain a steady state condition. Potentiodynamic polarization measurements were performed from −300 mV vs. OCP to +500 mV vs. OCP with a scanning rate of 0.5 mV/s. The current density values were normalized to the exposed surface area. The corresponding mean values were used in the relative diagrams.

The microscopic examination of the samples was performed by Scanning Electron Microscopy (SEM) using a 20 kV JEOL 840A scanning electron microscope (SEM, Jeol Ltd., Akishima, Tokyo, Japan) equipped with an OXFORD INCA Energy Dispersive X-ray Spectroscopy (EDS) analyzer (Oxford Instruments Nanoanalysis, Oxford, UK) and the INCA 18D 4.15 software that enabled point microanalysis and linear microanalysis of the area of interest. The phase identification was accomplished by X-ray diffraction (XRD) using 2-circles Regaku Ultima+ diffractometer (CuKα radiation, 40 KV, 30 mA) with Bragg–Brentano (BB-XRD, Rigaku Corporation, Shibuya-Ku, Tokyo, Japan).

3. Results and Discussion

3.1. Structure of Mg and Al Coatings

In Figure 1a, the cross section of the Mg coating deposited at 550 °C for 2 h is presented. The main remarks are that the coating has significant thickness of approximately 25 μm. While it is characterized by high homogeneity, as no cracks and porous areas are detected, the coating has two distinguishing layers. EDS line scanning analysis (Figure 1b) on these layers revealed that the inner layer contains 16 wt.% Mg, while the outer layer contains 44 wt.% Mg. Moreover, the thickness of the inner layer is 5 μm and the outer layer has an average thickness of 20 μm.
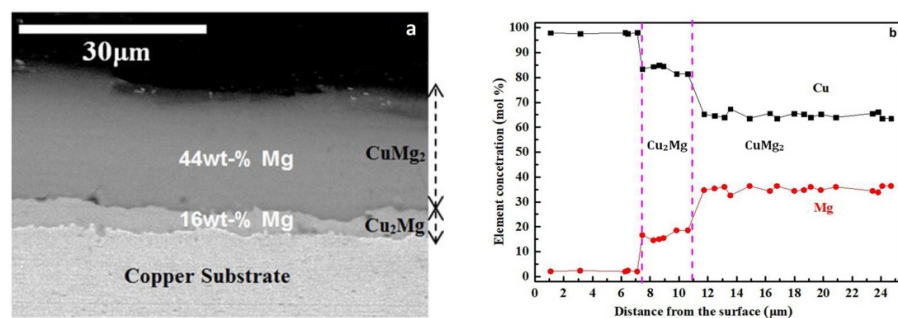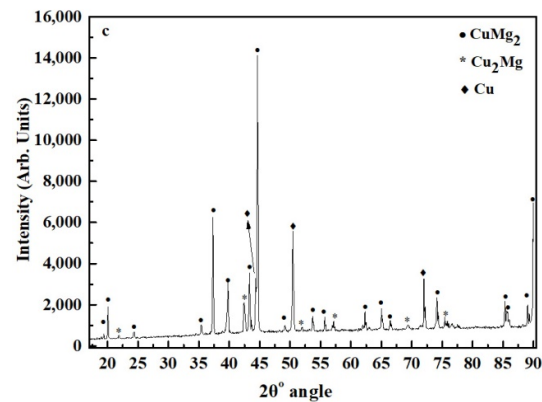
Figure 1. SEM micrograph of Mg pack coatings formed on copper at 550 °C for 2 h (**a**), corresponding Energy Dispersive Spectroscopy (EDS) line scanning (**b**) and XRD pattern (**c**) (The identification was accomplished by using the following JCPDS Cards: #65-1116 for $CuMg_2$, #77-1178 for Cu_2Mg and #85-1326 for Cu).

XRD analysis identified the existence of two distinct phases corresponding to the Cu_2Mg and to the $CuMg_2$ (Figure 1c). Combining these results with those of the EDS analysis, it is concluded that the inner layer is Cu_2Mg and the outmost layer is the $CuMg_2$ phase. This layer topography is also confirmed from the results of Ref. [24], in which it was found that for very short deposition time (30 min) the coating had one single layer corresponding to Cu_2Mg; for longer holding times, the $CuMg_2$ phase appeared over Cu_2Mg.The formation of these phases is the result of a two-step chemical procedure. In the beginning, Mg diffuses in the copper substrate which results to the formation of the $MgCu_2$ phase. The $MgCu_2$ increases as Mg diffusion continues through the Cu_2Mg. Moreover, some of the Mg ions do not reach the copper substrate but enrich the upper areas of the Cu_2Mg phase and transform it to $CuMg_2$. The rate of the formation of $CuMg_2$ increases as the thickness of the $MgCu_2$ grows, because the Mg ions have to traverse a bigger distance to reach Cu. After a particular point, the formation of extra $MgCu_2$ amounts is insignificant and that is the reason the $CuMg_2$ layer has bigger thickness than the inner Cu_2Mg layer.

The same characterization procedure was followed for the Al coated samples. In Figure 2a the coatings formed at 550 °C for 2 h is presented. In this case, a single phase 12 μm thick film is created, with similar homogeneity as the Mg coating as no cracks or pores were observed in its structure. EDS point microanalysis showed that the average Al concentration in the coating is 16 wt.% and the Cu is 84 wt.%. One single phase was traced in the XRD diffraction pattern corresponding to the Al_4Cu_9 (Figure 2b). Concluding from all the structural results, thick and homogeneous coatings were formed in every case. Furthermore, the phases that were detected in both cases are reported to have little effect on the electrical properties of Cu, thus, they can be effectively used in electrical applications [11].
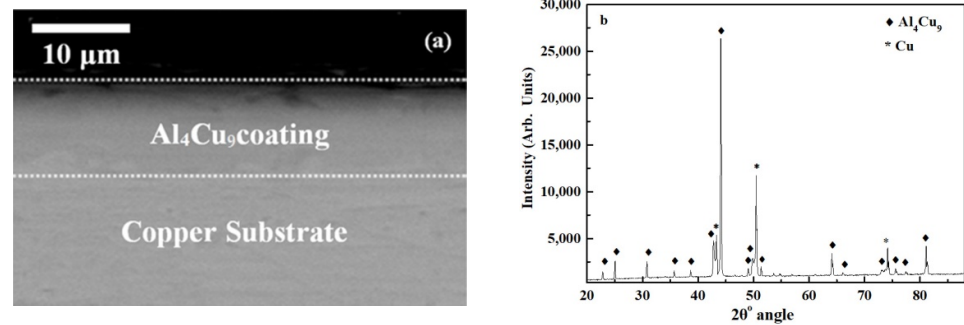
Figure 2. SEM micrograph of the Al coatings deposited at 550 °C for 2 h (**a**), and corresponding XRD pattern (**b**) (The identification was accomplished by using the following JCPDS Cards: #02-1254, # 65-3347 for Al_4Cu_9 and #04-0836 for Cu).

In the following section, these coatings are investigated for their corrosion and oxidation performance in order to be evaluated for applications working under harsh high temperature or marine environments.

3.2. High Temperature Oxidation

3.2.1. Dynamic Oxidation

From the non-isothermal oxidation of copper, it is revealed that the uncoated copper begins to oxidize at 200 °C, as from this temperature and on there is a considerable increase of the mass gain due to the oxide formation (Figure 3). After 400 °C the oxidation rate is high and continues to increase up to the end of the test (approx. 1000 °C)
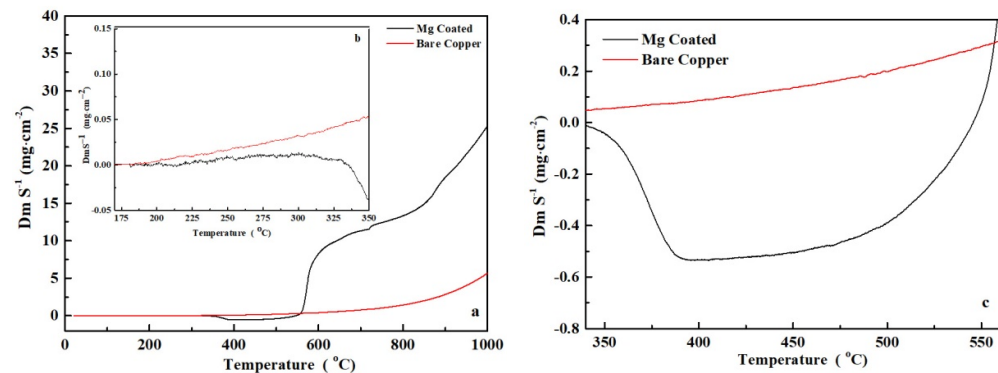
Figure 3. Mass gain graph of Mg coated and copper samples, after dynamic oxidation from room temperature up to 1000 °C (**a**) and focused graphs on the areas of interest (**b**,**c**).

In the same mass gain diagram, the Mg-coated sample does not oxidize until 560 °C (Figure 3b). This protection is attributed to the spontaneous formation of a thin and dense MgO oxide film (20–50 nm) on the surface as a result of the atmospheric air exposure [26,27]. Moreover, $Mg(OH)_2$ is also formed, as a result of the high affinity of Mg to the atmospheric humidity, on the surface of the samples. At 350 °C a drop of mass gain occurs (Figure 3c), which is due to the decomposition of $Mg(OH)_2$. For temperatures over 380 °C the $Mg(OH)_2$ destabilizes [26] and is totally transformed to amorphous MgO following Equation (1):

$$Mg(OH)_2 \rightarrow MgO + H_2O \tag{1}$$

This amorphous scale gradually grows with the increase of temperature and acts as a barrier to the aggressive environment up to 460 °C. From that point it begins to be less

protective, and a low-rate oxidation of the underlying coating begins. Over 560 °C, and especially over 600 °C, a dramatic mass gain is observed as a result of the high-rated oxidation of the sample. This change is mostly attributed to the residual stresses created in the oxide scale, which can provoke the creation of cracks in their structure. These stresses result from the difference between the crystal structure of the oxide and the coating material and from the growth mechanism of the scale based on the theory of Pilling-Bedworth ratio (PBR) for metals [28,29]. The PBR ratio in this case is:

$$PBR_{metal\ alloy} = \frac{Volume\ of\ a\ mole\ of\ MgO}{Volume\ of\ x\ atoms\ of\ Mg\ in\ the\ alloy} \tag{2}$$

When an oxide is formed on the surface of an alloy and not on pure metal, the metal with the most stable oxide is calculated for the factor V_{oxide}, here V_{MgO}. When the PBR ratio is higher than 1 then compressive stresses are created in the structure of the oxide scale, while when PBR< 1 then tensile stresses are created. The magnitude of these stresses is proportionate to the difference PBR−1.

In the herein case, the oxide formation is expressed from the chemical equation:

$$2Mg + O_2 \rightarrow 2MgO \tag{3}$$

The volume of 1 mole of MgO is:

$$V_{MgO} = \frac{W}{d} = \frac{40.03g}{3.58\ ^g/_{cm^3}} = 11.181\ cm^3 \tag{4}$$

where, W is the weight and d the density of 1 mole of oxide, respectively. Considering that there is no Cu-rich area formed underneath the MgO oxide, the volume of Mg moles in the alloy which oxidize forming MgO can be calculated from the expression [28]:

$$Volume\ of\ x\ moles\ Mg\ in\ alloy = \left(\frac{x}{u+v}\right) \times N \times V_{Mg_2Cu} \tag{5}$$

where, x is the moles of Mg required for the formation of MgO (Equation (3)) which is 2, N is Avogadro's number and u, v are the number of moles of every element in the Mg$_2$Cu alloy (surface layer of the as deposited coating), thus $u = 2$ and $v = 1$. From the JCPDS card #651116 and given that Mg$_2$Cu belongs to the orthorhombic Fddd system, the volume of the Mg$_2$Cu unit cell is:

$$V_{cell} = \frac{a \times b \times c}{4} = \frac{0.904 \times 10^{-7} \times 0.5275 \times 10^{-7} \times 1.838 \times 10^{-7}}{4}$$

$$V_{cell} = \frac{0.876 \times 10^{-21}}{4} = 0.219 \times 10^{-21} cm^3$$

where, a, b, c: lattice constants of the unit cell.

The volume of Mg in the Mg$_2$Cu molecule is [28]:

$$V_{Mg_2Cu} = \frac{V_{cell}}{n} = \frac{0.219 \times 10^{-21}}{4} = 0.05475 \times 10^{-21} cm^3$$

n is the number of atoms per unit cell in Mg$_2$Cu (Fddd system).

From Equation (5), the volume of $x = 2$ moles of Mg that oxidize is:

$$Volume\ of\ 2\ moles\ of\ Mg\ in\ alloy = \frac{2 \times 6.02 \times 10^{23} \times 0.05475 \times 10^{-21}}{3} = 21.984\ cm^3$$

As a result, the PBR ratio (Equation (2)) is:

$$PBR = \frac{11.181}{21.984} = 0.5085$$

Since PBR < 1, it is concluded that tensile stresses are created at the interface between the alloyed coating (Mg$_2$Cu) and the oxide scale. Thus, with the increase of the oxidizing temperature, the PBR ratio decreases further and more intense tensile stresses are creat-

ed. As a result, in the structure of the oxide scale more cracks are formed, providing easy paths for the aggressive agents to reach the coating and the copper substrate at longer exposure periods. The degradation of the coating occurs wherein a porous white oxide film grows over the surface, which stabilizes the oxidation rate at a lower value for the temperature range from 600 to 800 °C [12,28]. At 800 °C, the tensile stresses are so intense that it drives to the total collapse and delamination of the oxide scale, while a significant fraction of the Mg-Cu coating also oxidizes, leading to non-protective conditions of the Cu substrate.

The Al coated samples were found to be much more resistant under non-isotheral high temperature oxidation conditions. In Figure 4, the graph of mass gain vs. oxidation temperature is presented, in which it is revealed that, up to 650 °C, the sample does not oxidize as there is not any mass gain recorded. From this temperature, the oxidation rate slightly increases, until the temperature reaches 850 °C. After the latter temperature, the rate increases dramatically, which can result to the total deterioration of the coating and the substrate for long exposure periods. The stability of the coating up to 850 °C is attributed to the high affinity of Al to oxygen, which results in the formation of a very stable, thin and adhesive oxide on the top of the coating (Equation(6)). This scale acts as a barrier to the diffusion of oxygen in the coating. The grade of protection of this thin layer is relative to the Al concentration in the coating and of the oxidation temperature [16]. Thus, over 850 °C, this layer begins to destabilize; the rate of destabilization increases dramatically after 900 °C for 28 wt.% Al used in this case.

$$2Al + \frac{3}{2}O_2 = Al_2O_3 \tag{6}$$
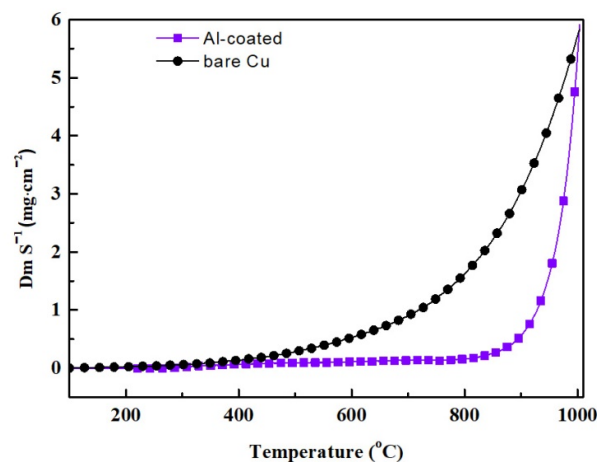
Figure 4. Mass gain graph of Al coated and copper samples, after dynamic oxidation from room temperature up to 1000 °C.

Comparing with the bare copper substrate, it is concluded that the Al coating provides superior protection to the substrate which can safely work under high-temperature aggressive environments.

Comparing the two types of coatings, the protection provided by the Al coatings is much better, as the samples with Mg coatings begin to oxidize 360 °C higher than Cu bare samples, while Al coated ones begin to oxidize 450 °C higher than Cu. As a conclusion, Al-coated components can be safely used up to 800–850 °C while Mg deposited components can be used in more moderate temperature, up to 450–500 °C. In any case, both limits can serve most of the application referred in the introduction.

3.2.2. Isothermal Oxidation

In order to examine the durability of both coatings under prolonged exposure periods and make a complete examination of the oxidation by thermal analysis, the samples were examined under constant temperatures for 6 h.

The Mg-coated sample was held under 550, 600, 650 and 700 °C dry air environment. As concluded from the dynamic oxidation of this sample in Figure 3, 550 °C is the temperature at which the oxidation was recorded at very low rate; 600 °C corresponds to the middle rate oxidation before the steep increase of the mass gain in the mass gain; and finally 650 and 700 °C are oxidation temperatures corresponding to oxidation conditions after this temperature point.

The results of the isothermal oxidations are illustrated in Figure 5 in the diagram of the mass gain vs. time (*t*). It is revealed that from the lowest oxidation temperatures (550, 600 °C) the samples have similar behavior; for the first minutes of exposure a linear increase of the mass gain is observed and afterwards the mass gain makes a plateau at which the oxidation rate is insignificant and the coating is highly protective to the substrate. For the higher oxidation temperatures (650, 700 °C) the rate of the mass gain is also linear in the first minute of exposure but afterwards this rate decreases but remains linear up to the end of the exposure but at a considerably lower rate. For further examination of the curves, the diagrams of mass gain vs. $t^{0.5}$ are presented in Figure 6a,b.
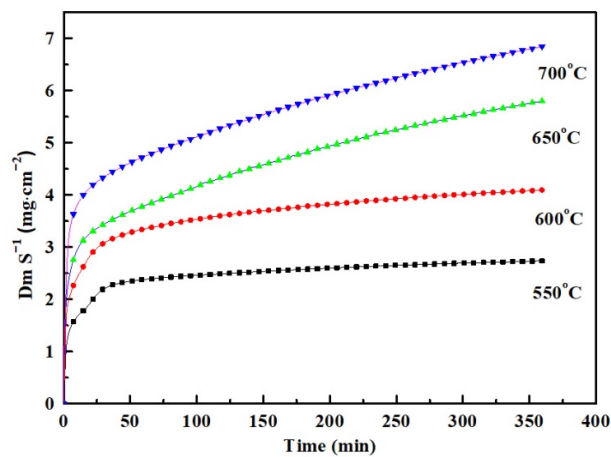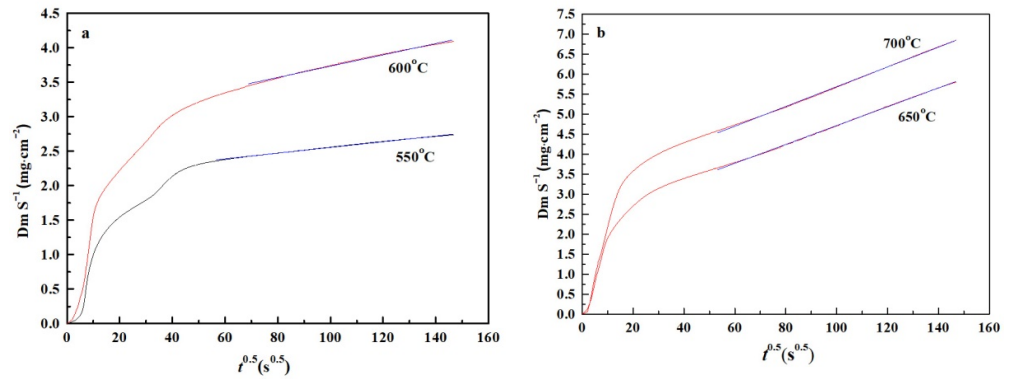

Figure 5. Mass gain graph of the Mg coated samples, after isothermal oxidation at 550, 600, 650, 700 °C.

From these graphs, it is concluded that, ignoring the first minutes of exposure, the oxidation rate can be described by a linear fitting with different slope for 550/600 °C and for 650/700 °C. As a result, the mass gain (Dm) and so oxidation follow the parabolic law vs. time (*t*), which is [30,31]:

$$Dm^2 = k_P \times t \tag{7}$$

k_P: is a rate constant which incorporates the rest of the factors affecting the phenomenon (see Equation (8)).

Figure 6. Mass gain vs.$t^{0.5}$ graph of the Mg coated samples, after isothermal oxidation at (**a**) 550, 600 °C and (**b**) 650, 700 °C.

The first ignored minutes of oxidation correspond to the formation of a protecting oxide scale, which provides passivation on the surface. After this step, the oxidation proceeds by ion diffusion in the coating. Thus, the constant of the mass gain rate (k_P) can be calculated from this step of the test (linear part of Figure 6). The results are presented in Table 1.

**Table 1.** Values of the constant of the mass gain rate (k_P) of Mg coated samples for 550, 600, 650, 700 °C.

T/°C	$k_p/\Delta m \times S^{-1} \times t^{-0.5}$
550	41.3×10^{-4}
600	82×10^{-4}
650	205.2×10^{-4}
700	246.9×10^{-4}

The calculation of the activation energy of the reactions was realized by the use of Arrhenius law, which is expressed by the equation:

$$k_P = k_0 \times e^{(-\frac{E}{RT})} \tag{8}$$

where, k_0 is the pre-exponential factor, E is the apparent activation energy, R is the gas constant and T is the absolute temperature.

Thus, the activation energy E was calculated from the slope of the $\ln[k_P(T)]$ vs. $1000/T$ (Figure 7) using the correlations [32–34] Dm^2 vs. $t^{0.5}$. The activation was finally calculated 86.2 kJ/mol.
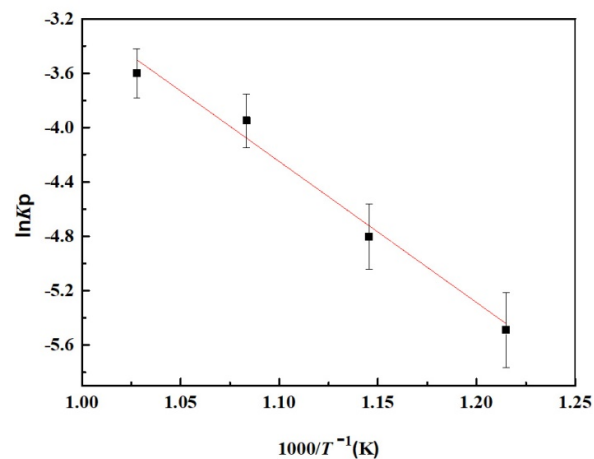
**Figure 7.** Graph of dependence of the parabolic oxidation rate constant from temperature for Mg coatings.

The Al coated sample was held under 800, 850, 900 and 950 °C in dry air environment. Following the same way of thinking with Mg coated samples and concluding from Figure 4, 800 °C is the temperature at which the oxidation was recorded at very low rate. Further, 850 °C corresponds to the middle rate oxidation. Finally, 900 °C corresponds to the critical temperature after which the oxidation rate increases dramatically, and at 950 °C the samples have significant oxidation rate. The graphs corresponding to isothermal measurements are presented in Figure 8.
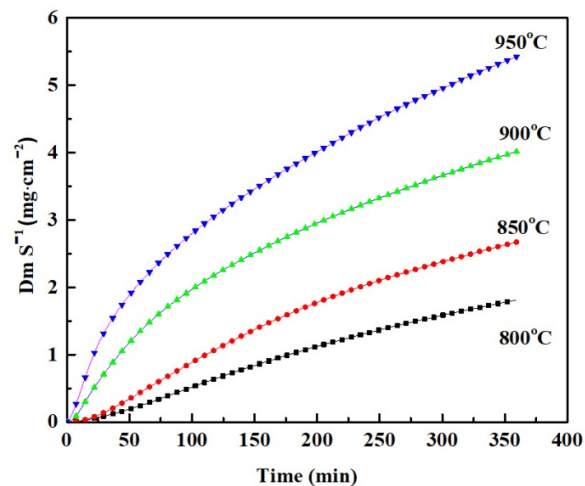
Figure 8. Mass gain graph of the Al coated samples, after isothermal oxidation at 800, 850, 900, 950 °C.

From these graphs it is concluded that, at the lowest temperatures (800, 850 °C), the curves have approximately similar behavior; at the first steps of exposure the mass gain increases linearly, and afterwards it tends to a plateau and the rate of oxidation stabilizes to a very low constant rate. At higher oxidation temperatures (900, 950 °C) the mass gain rate is also linear and has much longer duration comparing with 800 and 850 °C curves. Afterwards, the rate decreases but still has a significant value. Furthermore, the curves do not seem to have the tension of making any plateau. The behavior of these last curves can be attributed to the too high oxidation temperature, which is detrimental for any protective scale formed on the surface of the samples.

In Figure 9 the diagrams of the mass gain vs. $t^{0.5}$ are presented and it is equally revealed that, ignoring the first time-limited step of oxidation, the remaining phenomenon follows the parabolic law of Equation (7) as a result of ion diffusion.
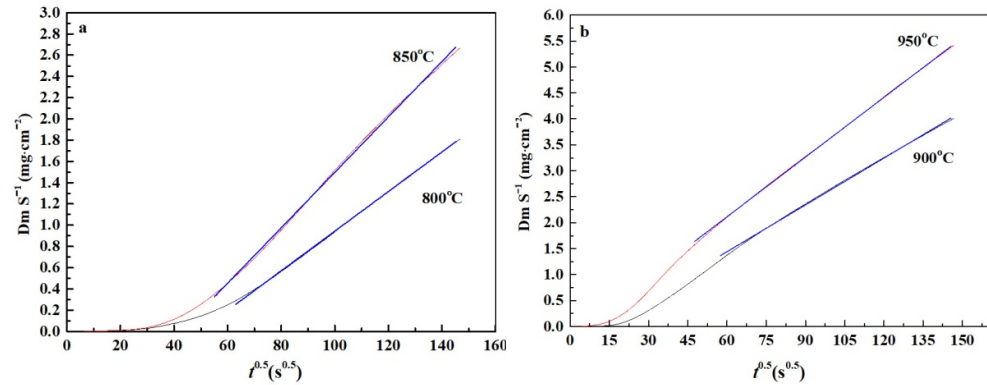

Figure 9. Mass gain vs. $t^{0.5}$ graph of the Al coated samples, after isothermal oxidation at (**a**) 800, 850 °C and (**b**) 900, 950 °C.

The constant of the mass gain rate (k_P) was calculated from the linear part of each graph of Figure 9 and is presented in Table 2.

Table 2. Values of the constant of the mass gain rate (k_P) of Al coated samples for 800, 850, 900, 950 °C.

$T/°C$	$k_p/\Delta m \times S^{-1} \times t^{-0.5}$
800	185.2×10^{-4}
850	261.2×10^{-4}
900	300.6×10^{-4}
950	385.7×10^{-4}

Activation energy E was calculated from Equation (2) and from the slope of the $\ln[k_P(T)]$ versus $1000/T$ graph (Figure 10). The activation was finally calculated at 52.105 kJ/mol.
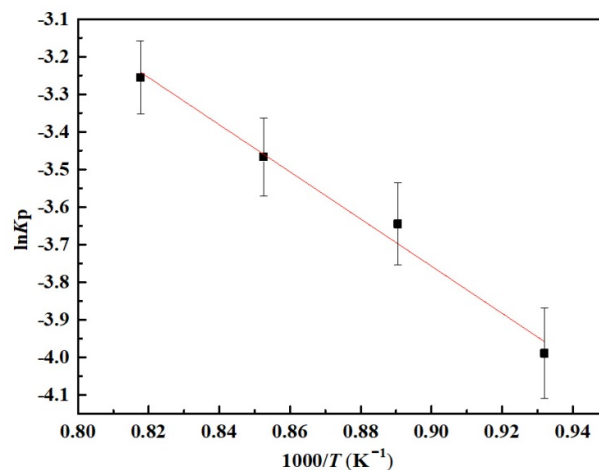

Figure 10. Graph of dependence of the parabolic oxidation rate constant from temperature for Al coatings.

The low value of the activation energy of both coatings is mainly attributed to the high affinity of Mg and Al to oxygen. However, the chemical result of this reaction is the creation of protective scales, which hinders the diffusion of oxygen in the underlying coating and substrate, assuring safe, long-lasting service life compared to the bare Cu samples. Comparing the two coatings, it can be assessed that Al coatings have superior protection from Mg because, in dynamic oxidation, it begins to oxidize at much higher temperature and with significantly lower rate. Furthermore, in isothermal oxidations Al coatings have approximately same mass gain with Mg ones but at a temperature 250 °C higher.

3.3. Electrochemical Corrosion

The samples were also examined under electrochemical corrosion in order to estimate their durability in marine atmospheres under the effect of oxygen and chlorine ions.

The open circuit potential (OCP), E_{OCP}, of all samples in 3.5 wt.% NaCl aqueous solution after a period of 60 min are shown in Figure 11. It can be seen that, compared to pure copper potential, the coated samples have less electronegative E_{OCP} as reported in Table 3. These differences are related to the different nature of the materials (Cu, phases of Mg or Al) directly exposed to the solution. It should be noted that the high homogeneity of the coatings and the absence of cracks and porous areas in their structure is a first indication of the protection of copper from the corrosive environment.
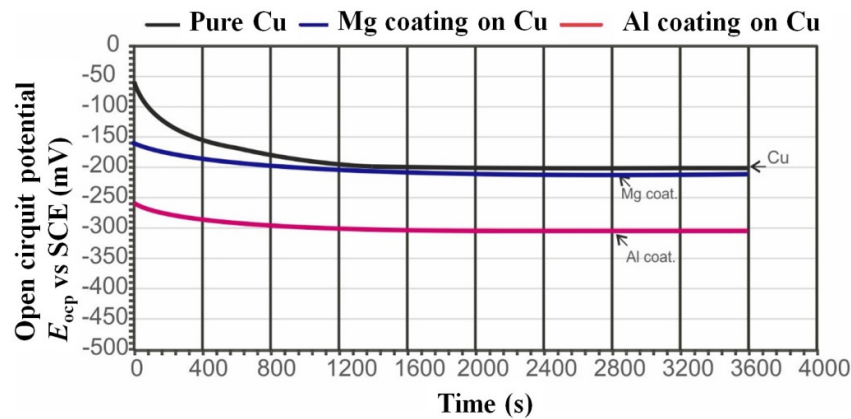
Figure 11. Open circuit potential (OCP) curves of uncoated and coated samples in 3.5 wt.%NaCl solution at 25 °C.

The potentiodynamic polarization diagrams of the uncoated and coated samples are presented in Figure 12. In the cathodic part of the polarization curves, two regions can be clearly observed. The first one represents the reduction of dissolved oxygen in the solution and the second one the reduction of hydrogen. The corrosion potentials (E_{corr}), the corrosion current densities (i_{corr}) and the anodic/Cathodic Tafel slopes are reported in Table 3. The differences between E_{OCP} and E_{corr} values probably indicate a chemical change at the working electrodes surfaces as a result of alkalization from cathodic reactions occurring during the potentiodynamic scan [35]. These parameters were estimated by taking into consideration several zones from 50 to 200 mV to optimize the fitting of the Tafel slopes. Additionally, in Table 3 the corrosion rates of the samples are reported calculated [33,36] by Equation (9):

$$\text{Corrosion rate} = (0.13 \times I_{corr} \times E.W.)/d \qquad (9)$$

where, *E.W.* is the equivalent weight of the oxidized element in g (63.5/2 Cu, 26.98/3 Al and 24.3/2 Mg) and *d* is the density of the corroded specimens in g/cm^3.

Table 3. OCP (E_{OCP}), corrosion potentials (E_{corr}), corrosion current densities (i_{corr}), Tafel slopes and corrosion rates of uncoated and Mg, Al coated samples in 3.5 wt.% NaCl aqueous solution at 25 °C(mean values with standard deviation for potentials <7% and for current densities <5%).

Type of Sample	E_{OCP} (mV vs. SCE)	E_{corr} (mV vs. SCE)	i_{corr} ($\mu A/cm^2$)	β_a	$-\beta_c$	Corrosion Rate (mpy)
Pure copper	−200	−170	3	46	53	1.38
Mg coat.	−210	−220	0.9	58	56	0.9
Al coat.	−311	−330	1	83	80	0.82

From the results it is concluded that the corrosion rates follow the same trends as i_{corr}. The corrosion rates of the coated samples are lower than that of the copper uncoated samples. Apart from that, by examining the anodic regions of the potentiodynamic curves (Figure 12), it is revealed that the current of the uncoated samples increases rapidly after E_{corr}.
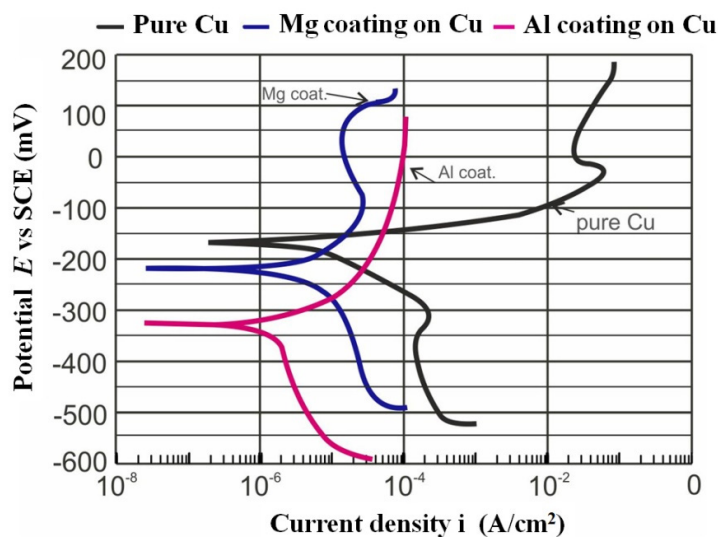
Figure 12. Potentiodynamic polarization curves of uncoated and coated samples in 3.5 wt.% NaCl solution at 25 °C.

For the Mg coatings and pure copper samples, a passive-like region, where current densities are reduced, can be observed (Figure 12) due to the formation of any corrosion products like $Mg(OH)_2$ and Cu_2O or CuO on them, whereas the active dissolution for the Al coatings continues approaching a stable value of current density (around 10^{-4} A/cm^2) due to the formation of Al_2O_3 on the surface [37,38]. Both coated samples are found to have similar corrosion resistance and relative significantly higher than the unprotected copper coupons.

4. Conclusions

From the results of this scientific examination, it is concluded that the structure morphology of Mg and Al coatings deposited by pack cementation, is compact with no cracks and areas with pores. For the case of Mg deposition, the coating has two distinct layers corresponding to $MgCu_2$(inner layer) and Mg_2Cu (outer layer). For the case of Al deposition, the coatings have one single layer corresponding to the Al_4Cu_9 phase. The Al coatings were found to be remarkably more resistant in high temperature air environments than Mg coatings. However, both coatings are much more durable than the unprotected copper substrate. From the corrosion tests corresponding to marine environment, it is concluded that both Al and Mg coatings have similar and elevated corrosion

resistance as compared with copper substrate, and can offer long-term protection when working under similar conditions.

Institutional Review Board Statement: Not applicable.

Informed Consent Statement: Not applicable.

Conflicts of Interest: The authors declare no conflict of interest. The funders had no role in the design of the study; in the collection, analyses, or interpretation of data; in the writing of the manuscript, or in the decision to publish the results.

Reference

1. Sozer, E.; Jiang, C.; Gundersen, M.; Umstattd, R. Quantum efficiency measurements of photocathode candidates for back-lighted thyratrons. *IEEE Trans. Dielectr. Electr. Insul.* **2009**, *16*, 993–998.
2. Kim, K.; Norton, D.; Christen, D.; Budai, J. Formation of oxidation-resistant Cu-Mg coatings on (001) Cu for oxide superconducting tapes. *Surf. Coat. Technol.* **2008**, *202*, 5136–5139.
3. El-Feky, H.; Helal, N.; Negem, M. Electrochemical behavior of some copper alloys in sulfuric acid solutions. *Mater. Corros.* **2009**, *61*, 599–610.
4. Ptil, S.; Sainkar, S.; Patil, P. Poly(o-anisidine) coatings on copper: Synthesis, characterization and evaluation of corrosion protection performance. *Appl. Surf. Sci.* **2004**, *225*, 204–216.
5. Lachowicz, M.M. A metallographic case study of formicary corrosion in heat exchanger copper tubes. *Eng. Fail. Anal.* **2020**, *111*, 104502.
6. Shinde, V.; Sainkar, S.; Patil, P. Corrosion protective poly(o-toluidine) coatings on copper. *Corros. Sci.* **2005**, *47*, 1352–1369.
7. Tan, A.; Soutar, A. Hybrid sol-gel coatings for corrosion protection of copper. *Thin Solid Film* **2008**, *516*, 5706–5709.
8. Rahman, A.; Jayaganthan, R.; Prakash, S.; Chawla, V.; Chandra, R. Cyclic high temperature oxidation behaviour of sputtered Cr/Al multilayer coatings on superalloy. *Surf. Eng.* **2011**, *27*, 393–401.
9. Chaliampalias, D.; Andronis, S.; Stergioudis, G.; Tsipas, D.; Vourlias, G.; Pavlidou, E. Deposition of multilayer NiCrBSiFe and Al coatings on low carbon steels. In Proceedings of the MC2011 Microscopy Congress, Kiel, Germany, 28 August–2 September 2011.
10. Suwwan de Felipe, T.; Murarka, S.P.; Bedell, S.; Lanford, W.A. Capacitance-voltage, current voltage, and thermal stability of copper alloyed with aluminum or magnesium. *Thin Solid Films* **1998**, *335*, 49–53.
11. Arcot, B.; Murarka, S.P.; Clevenger, L.A.; Hong, Q.Z.; Ziegler, W.; Harper, J.M.E.; Intermetallic formation in copper/magnesium thin films-kinetics, nucleation and growth, and effect of interfacial oxygen. *J. Appl. Phys.* **1994**, *76*, 5161.
12. Zhu, Y.F.; Lu, H.M.; Jiang, Q.; Mimura, K.; Isshiki, M.; Effect of alloying Mg on corrosion resistance of Cu at high temperature. *J. Electrochem. Soc.* **2007**, *154*, C153–C158.
13. Zhao, X.Q.; Han, Y.F.; Liu, B.X. Modification of oxidation resistance of copper films by shallow implantation. *J. Appl. Phys.* **2001**, *90*, 1638.
14. Chiang, K.-T.; Kallenborn, K.J.; Yuen, J.-L. Aluminization of copper for oxidation protection. *Surf. Coat. Technol.* 1992, *52*, 135-139.
15. Gembalski, S. Diffusion aluminizing of steel, cast iron, copper and titanium. *Met. Sci. Heat Treat.* **1967**, *9*, 646–651.
16. Abd El-Azim, M.E.; Soliman, H.M. Pack aluminizing of copper. *J. Mater. Technol.* **1997**, *13*, 127–132.
17. Shi, Z.; Wang, D. Surface dispersion hardening Cu matrix alloy. *Appl. Surf. Sci.* **2000**, *167*, 107–112.
18. Çorlu, B.; Ürgen, M. Modification of copper surfaces with cathodic arc aluminum plasma. *Surf. Coat. Technol*. **2010**, *205*, 540–544.

19. Ding, P.J.; Wang, W.; Lanford, W.A.; Hymes, S.; Murarka, S.P. Thermal annealing of buried Al barrier layers to passivate the surface of copper. *Appl. Phys. Lett.* **1994**, *65*, 1778.

20. Lee, K.S.; Kwon, Y.N. Solid-state bonding between Al and Cu by vacuum hot pressing. *Trans. Nonferrous Met. Soc. China* **2013**, *23*, 341−346.

21. Stathokostopoulos, D.; Chaliampalias, D.; Pavlidou, E.; Hatzikraniotis, E.; Stergioudis, G.; Paraskevopoulos, K.M.; Vourlias, G. Formation of Mg$_2$Si thick films on Si substrates using pack cementation process. In Proceedings of the AIP Conference, Thessaloniki, Greece, 28–30 September 2011; pp. 203–206.

22. He, M.; Liu, L.; Wu, Y.; Zhong, C.; Hu, W. Influence of microstructure on corrosion properties of multilayer Mg-Al intermetallic compound coating. *Corros. Sci.* **2011**, *53*, 1312–1321.

23. Cultrera, L.; Pereira, A.; Ristoscu, C.; Clozza, A.; Tazzioli, F.; Vicario, C. Pulsed laser deposition of Mg thin films on Cu substrates for photocathode applications. *Appl. Surf. Sci.* **2005**, *248*, 397–401.

24. Stathokostopoulos, D.; Chaliampalias, D.; Pavlidou, E.; Chrissafis, K.; Stergioudis, G.; Patsalas, P.; Vourlias, G. Protection of Cu components with Mg and Al coatings deposited by pack cementation. *Surf. Eng.* **2014**, *30*, 886–892.

25. Stathokostopoulos, D.; Chaliampalias, D.; Pavlidou, E.; Vourlias, G.; Stergioudis, G. Structural study of magnesium coatings on copper substrates by pack cementation. *Solid State Phenom.* 2013, *203–204*, 9–12.

26. Nordlien, J.; Ono, S.; Masuko, N.; Nisancioglu, K. A TEM investigation of naturally formed oxide films on pure magnesium. *Corros. Sci.* **1997**, *39*, 1397–1414.

27. Eliezer, D.; Alves, H. Corrosion and oxidation of magnesium alloys. In *Handbook of Materials Selections*; Kurtz, M., Ed.; Wiley: New York, NY, USA, 2002; pp. 267–292.

28. Xu, C.; Gao, W. Pilling-bed worth ratio for oxidation of alloys. *Mater. Res. Innov.* **2000**, *3*, 231–235.

29. Makar, G.L.; Kruger, J. Corrosion of magnesium. *Int. Mater. Rev.* **1993**, *38*, 138–153.

30. Zhang, S.; Pisch, A.; D'hemle, F. Oxidation of refractory intermetallic compounds: Kinetics and thermodynamics. *Philos. Mag. A* **1996**, *73*, 709–722.

31. Pieraggi, B. Calculations of parabolic reaction rate constants. *Oxid. Met.* **1987**, *27*, 177–185.

32. Chaliampalias, D.; Vourlias, G.; Pavlidou, E.; Chrissafis, K. Examination of the oxidation resistance of Cr-Mo-V tool steel by thermal analysis. *J. Therm. Anal. Calorim.* **2011**, *108*, 677–684.

33. Pieraggi, B.; Rapp, R. Chromia scale growth in alloy oxidation and the reactive element effect. *J. Electrochem. Soc.* **1993**, *140*, 2844–2850.

34. Kofstad, P. *High Temperature Corrosion*, 3rd ed.; Elsevier: New York, NY, USA, 1988; pp. 250–281.

35. Vogiatzis, C.; Skolianos, S. Electrochemical evaluation of sintered aluminium–ceramic cenospheres composites. *Corros. Eng. Sci. Technol.* **2017**, *52*, 90–98.

36. Revie, R.W.; Elboujdaini, M.; Ghali, E.; Yousri, E.; An electrochemical method to control the anodizing process. In *Materials Performance Maintenance*; Elsevier: Toronto, ON, Canada, 1991.

37. Song, G.L. *Corrosion of Magnesium Alloys*; Wood head Publishing Limited: Cambridge, UK, 2011; pp. 117–165.

38. Nagiub, A. Evaluation of corrosion behavior of copper in chloride media using electrochemical impedance spectroscopy (EIS). *Port. Electrochim. Acta* **2005**, *23*, 301–314.